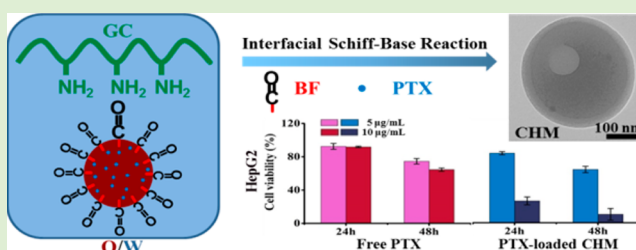


# Adaptive Chitosan Hollow Microspheres as Efficient Drug Carrier

Ya-nan Fu,<sup>†</sup> Yongsan Li,<sup>†,‡</sup> Guofeng Li,<sup>†</sup> Lei Yang,<sup>§</sup> Qipeng Yuan,<sup>†</sup> Lei Tao,<sup>‡,ⓑ</sup> and Xing Wang<sup>\*,†,ⓑ</sup><sup>†</sup>Beijing Laboratory of Biomedical Materials, Beijing University of Chemical Technology, Beijing 100029, People's Republic of China<sup>‡</sup>The Key Laboratory of Bioorganic Phosphorus Chemistry and Chemical Biology (Ministry of Education), Department of Chemistry, Tsinghua University, Beijing 100084, People's Republic of China<sup>§</sup>Cancer Institute and Hospital, Peking Union Medical College and Chinese Academy of Medical Science, Beijing 100021, People's Republic of China

## Supporting Information

**ABSTRACT:** Smart drug carrier with function-oriented adaptations is highly desired due to its unique properties in medical applications. Herein, adaptive chitosan hollow microspheres (CHM) are fabricated by employing interfacial Schiff-base bonding reaction. Hydrophilic macromolecules of glycol chitosan are fixed at the oil/water interface through numerous hydrophobic small molecules of borneol 4-formylbenzoate, forming the CHM with a positively charged surface and lipophilic cavity. These CHM have an average size of 400–1000 nm after passing through the 0.22  $\mu\text{m}$  apertures of filter paper. This phenomenon combined with SEM measurements demonstrates its remarkable shape-adaptive behavior. Furthermore, the CHM present a pH-dependence of structural stability. When pH value reduces from 7.06 to 5.01, the CHM begin to lose their integrity. All those characteristics make the CHM an intelligent drug carrier, especially for water-insoluble anticancer drugs, paclitaxel (PTX) in particular. Both cell uptake and cell cytotoxicity assays suggest that the PTX-loaded CHM are highly efficient on HepG2 and A549 cells. Therefore, rather than most of the traditional materials, these adaptive CHM show great potential as a novel drug carrier.



## 1. INTRODUCTION

A serious challenge is posed to lipophilic anticancer drugs. Their well-known poor water solubility greatly limited their efficacy when using those molecules to approach the nidus.<sup>1</sup> In addition, high toxicity of free drugs, low bioavailability and the drug resistance are also problems.<sup>2,3</sup> To address these issues, a wide variety of drug carriers have been proposed.<sup>4–11</sup> Till now, numerous drug carrier systems, such as liposomes,<sup>6</sup> polymeric micelles,<sup>7</sup> microspheres or microcapsules,<sup>8,9</sup> nanoemulsions,<sup>10</sup> and nanoparticles,<sup>11</sup> have become popular types in biomedical applications. Though each of them has unique characteristics, most of them are traditional materials with fixed form. Developing smart drug carrier especially with function-oriented adaptability is thus highly desired.

In recent years, polymeric microspheres have emerged as one promising drug carrier systems due to its obvious superiorities, such as easy tailorability of chemical compositions, precisely controlled size and surface properties, high efficiency, and low cost.<sup>12–14</sup> Their versatility have successfully endowed anticancer drugs with stable loading, targeting, controlled or responsive release, and so on.<sup>15–17</sup> Some hollow microspheres (microcapsules) can even not only further increase drug-loading efficiency, but also enhance stimuli-responsive ability.<sup>18</sup> Therefore, many methods, including emulsion cross-linking,<sup>19</sup> ionic gelation,<sup>20</sup> complex coacervation,<sup>21</sup> spray drying,<sup>22</sup> and self-assembly,<sup>23,24</sup> have been developed to design and prepare

polymer-based hollow microspheres based on biocompatible polymers and biomacromolecules.

Chitosan is a naturally alkaline polysaccharide with good biocompatibility, biodegradability, nontoxic, and transmembrane ability.<sup>25</sup> It has been widely used for many pharmaceutical and medical applications, such as implant surgeries,<sup>26</sup> protein or gene delivery,<sup>27,28</sup> and controlled release systems.<sup>29,30</sup> Chitosan can increase the permeability of cell membranes; its cationic property allows it to adhere to cell membranes more easily.<sup>31,32</sup> Therefore, many drug carriers are designed on the basis of chitosan and its derivatives.<sup>33–36</sup> Lehr et al.<sup>33</sup> chose squalene to covalently bind chitosan, the obtained amphiphilic polymer could spontaneously form particles by self-assembly and encapsulate several drugs. Chu et al.<sup>34</sup> developed core-shell chitosan microcapsules based on a cross-linking reaction of double emulsion of chitosan and terephthalaldehyde. The used microfluidic approach made monodisperse microcapsules, which displayed an acid-triggered burst release of hydrophobic drugs. All these cases demonstrated that chitosan and its derivatives are good candidates for drug carriers. And these works inspired us to construct smart drug carriers using dynamic Schiff-base,<sup>35,36</sup> because its remarkable pH-responsive capability, stable under neutral

Received: April 26, 2017

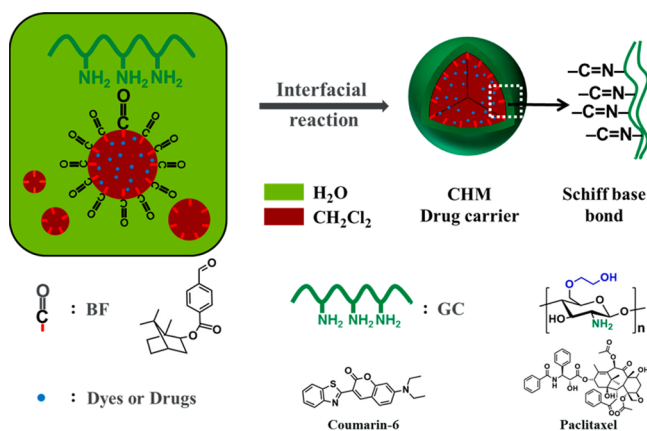
Revised: May 25, 2017

Published: May 30, 2017

conditions, and sensitive to hydrolysis under acidic conditions, is closely related to the inherent difference of pH between intracellular and extracellular environments or among different internal environments of human body.<sup>37</sup>

Herein, we contribute a new strategy to fabricate chitosan hollow microspheres (CHM) via an interfacial Schiff-base bonding reaction, as shown in Scheme 1. We employ numerous

**Scheme 1. Schematic Illustration of the Interfacial Schiff-Base Bonding Reaction That Is Designed between GC and BF Molecules in an Oil/Water Emulsion<sup>a</sup>**



<sup>a</sup>Hydrophobic drugs and dyes can be embedded in this CHM carrier.

hydrophobic small molecules of borneol 4-formylbenzoate (BF) to fix water-soluble hydrophilic macromolecules of glycol chitosan (GC) at the oil/water interface. The resulted interfacial complex is reversed to be insoluble in both water and organic solvents due to the big hydrophobic pendants ( $-\text{N}=\text{C}-\text{BF}$ ) on chitosan chains.<sup>38</sup> Since the aqueous phase is GC aqueous solution that form the shell of CHM, its outside should still be hydrophilic as well as GC itself, making it a good candidate for drug carrier. Remarkably, different to the cross-linking structures,<sup>34</sup> the bonding manner of the CHM endows this carrier more flexible and sensitive to surrounding environment, thus, indicating potential shape-adaptive and pH-responsive abilities. Moreover, the introduced borneol known as medical molecule has the physiological function to increase permeability of cell membrane.<sup>39,40</sup> Therefore, from both macro- and microscales, the CHM is an easy fabricated and smart carrier for tough anticancer drugs, with expected high efficacy potentially in injection therapy.

## 2. EXPERIMENTAL SECTION

**2.1. Reagents and Materials.** Glycol chitosan (GC, WAKO,  $M_w$  = 82 kDa up, degree of deacetylation: 85%), dichloromethane ( $\text{CH}_2\text{Cl}_2$ , 99%), 4-formylbenzoic acid (99%), *N,N*-dicyclohexylcarbodiimide (DCC, 99%), 4-(dimethylamino) pyridine (DMAP, 99%), paclitaxel (PTX, 99%), and 3-(4,5-dimethylazolyl-2)-2,5-diphenyl tetrazolium bromide (MTT) were purchased from Tokyo Chemical Industry (TCI). (–)-Borneol (99%), coumarin-6 (98%), and tetrahydrofuran (THF, 99.9%) were purchased from J&K Scientific. All the other reagents (AR grade) were used as received from Sinopharm. The mouse fibroblast cells (L929), the human hepatocarcinoma (HepG2) cells, and human nonsmall lung cancer (A549) cells were purchased from Cell Resource Center, IBMS, CAMS/PUMC, Beijing, China. Dulbecco's modified Eagle's medium (DMEM), Roswell Park Memorial Institute (RPMI) 1640 medium, fetal bovine serum (FBS), penicillin, and streptomycin were purchased from Gibco BRL (Gaithersburg, MD, U.S.A.).

**2.2. Synthesis and Characterization of BF.** BF was synthesized via a one-step esterification between borneol and 4-formylbenzoic acid, where DMAP and DCC were used as catalyst (Figure S1). This typical esterification results a yield of BF over 95%. BF was characterized by FT-IR (Figure S2):  $1725\text{ cm}^{-1}$  ( $-\text{C}=\text{O}$ ),  $1180\text{ cm}^{-1}$  ( $-\text{O}-\text{C}-\text{O}$ ); and  $^1\text{H NMR}$  (400 MHz, DMSO,  $\delta$ ; Figure S3): 0.8–0.9 (s, 9H,  $\text{CH}_3$ ), 1.0–2.3 (s, 7H,  $\text{CH}_2\text{CH}$ ), 8.08, 8.16 (d, 4H, Ph), 10.13 (s, 1H, CHO); and the GC-MS (Figure S4): in GC image (top), 16.01 min (single peak); in MS image (below), the fragments of the BF which were broken according to different rules determined that BF has no byproducts. All these results demonstrated that BF was synthesized successfully.

**2.3. Preparation and Characterization of the CHM.** The CHM was prepared via an interfacial Schiff-base bonding reaction at room temperature, as shown in Scheme 1. In brief, GC solution (1 wt % in deionized water) was used as water phase (W); oil phase (O) was  $\text{CH}_2\text{Cl}_2$  that contains BF (2.9 mg in 0.5 mL, 0.01 mmol). The volume ratio of W/O was fixed at 5:1. The O and pure water (1.68 mL) were first mixed under stirring at 1300 rpm for 6 h to obtain a primary emulsion. Then, GC solution (0.82 mL) was added in above system for another 2 h stirring at 1300 rpm. The final emulsion was obtained after stirring overnight to remove  $\text{CH}_2\text{Cl}_2$  completely. The CHM was obtained after passing through 0.22  $\mu\text{m}$  microporous membrane (Life Science Acrodisc 25 mm Syringe Filter) and being freeze-dried.

Coumarin-6 or PTX-loaded CHM was prepared following the procedure for the preparation of the CHM, where hydrophobic coumarin-6 (8.33  $\mu\text{g}$ ) or PTX (0.5 mg) was added to the BF solution (2.9 mg in  $\text{CH}_2\text{Cl}_2$ ) before the interfacial Schiff-base bonding reaction.

Scanning electron microscopy (SEM, S-4700 Hitachi) was used to observe the surface morphology and shape-adaptive transformation of the CHM. The freeze-dried samples were directly coating on conducting resin and treated by spray-gold. Transmission electron microscope (TEM, H-800 Hitachi) was performed to study core-shell interior structure of the CHM. The freeze-dried samples were redispersed in deionized water, 100  $\mu\text{L}$  of suspension was deposited on the surface of copper grid. The acceleration voltage for the SEM measurements was 15.0 kV. The acceleration voltage for the TEM measurements was 200 kV. The coumarin-6 loaded CHM was evaluated by fluorescence microscope that equipped with a CCD camera (BDS200-FL, TS 62, Instec, U.S.A.) at an excitation of 480 nm. One drop of freshly prepared emulsion was dripped on glass slide and observed immediately. Dynamic light scattering (DLS) and Zeta potential measurements were measured by Zetasizer Nano-ZS equipment (Malvern NanoSizer ZS2000). It is calculated from three measurements. Each sample was repeated six times. Confocal laser scanning microscopy (CLSM, Leica SPS, Germany) equipped with an argon/neon laser and a 63 $\times$  water immersion objective, was performed to observe 3D distribution of dyes in the CHM, and the real-time cellular uptake of the coumarin-6 loaded CHM. The measurement and image analysis were performed with Zeiss Zen Black software.

A UV-vis spectrophotometer (UV-2450, Shimadzu) was used to measure the drug loading efficiency (DLE), drug encapsulation efficiency (DEE), and in vitro PTX release of PTX-loaded CHM. DLE and DEE were calculated according to the following equations.<sup>41</sup>

$$\text{DLE}(\text{wt}\%) = \frac{(\text{amt of loaded PTX})}{(\text{amt of PTX} - \text{loaded CHM})} \times 100\%$$

$$\text{DEE}(\text{wt}\%) = \frac{(\text{amt of loaded PTX})}{(\text{initial amt of PTX})} \times 100\%$$

Briefly, the freshly prepared PTX-loaded CHM was dialyzed in deionized water for 24 h with a dialysis membrane ( $MWCO = 10$  kDa) to remove the nontrapped PTX. Then, 1 mL of sample was added into 20 mL of methanol with incubation for 24 h at 37  $^\circ\text{C}$ , following a sonication (2 h) and centrifugation progress (5000 rpm, 30 min) at room temperature, the concentration of PTX in solution was determined by UV-vis at 227 nm. A standard curve was made by pure PTX in methanol with different concentrations.

**2.4. pH-Responsive Behavior of the CHM.** The pH-responsive behavior of the CHM was analyzed in a series of PBS solutions (pH

range from 5.01 to 6.03, further to 7.06), which were used to simulate an internal biological environment.<sup>30–34</sup> The freeze-dried CHM was immersed in above-mentioned PBS solutions, respectively. The changes of morphology of the CHM under various pH values were recorded by optical microscope equipped with a CCD camera (BDS200-FL, TS 62, Instec., U.S.A.). A total of 10 min were used for this evaluation. In addition, the cryo-scanning electron microscope (cryo-SEM, FEI Helios NanoLab 600i) was employed to further study the stability of the CHM under various pH values at different time point from 2 to 24 h.

**2.5. In Vitro PTX Release.** In vitro release studies of PTX were conducted using a dialysis method. Briefly, 2 mL of PTX-CHM solution was added into a dialysis bag (MWCO = 10 kDa) soaked in 30 mL of PBS (pH 5.01, 6.03 or 7.06) containing 0.1% Tween 80 and incubated at 37 °C with gentle shaking.<sup>42</sup> At a predetermined time interval (from 0.5 to 48 h), 2 mL of samples in different pH medium were withdrawn and replaced with an equivalent volume of the corresponding fresh buffer solution, successively. The cumulative amount of PTX released from PTX-CHM in each buffer was quantified by its absorbance at 227 nm with a UV–vis spectrophotometer (UV-2450, Shimadzu) according to the standard curve.<sup>43</sup> The in vitro release experiments were carried out in triplicate.

**2.6. In Vitro Biocompatibility and Cytotoxicity Evaluation.** The biocompatibility of BF, GC, and the CHM blank was investigated with L929 cells. L929 cells were cultivated in RPMI 1640 that was supplemented with 10% FBS, 100 units mL<sup>-1</sup> penicillin and 100 µg mL<sup>-1</sup> streptomycin in humidified incubator of 95% air and 5% CO<sub>2</sub> at 37 °C. Typically, L929 cells were seeded in 96-well plates at the density of  $5 \times 10^3$  cells per well in 100 µL of RPMI 1640 medium, and then incubated at 37 °C for 24 h. Then equal volume fresh medium containing serial dilutions of BF (29 and 58 µg mL<sup>-1</sup>), GC (82 and 164 µg mL<sup>-1</sup>) and the CHM blank (0.86 and 1.72 mg mL<sup>-1</sup>, with the same GC or BF concentrations) to replace the solution in the plate ( $n = 6$ ). After 24 and 48 h of incubation, the cell viability was determined by MTT colorimetric assays, where 20 µL of MTT solution (5 mg mL<sup>-1</sup>) was added to every well and incubation for 4 h at 37 °C. After removing the solution, the formazan crystals in each well were dissolved by 150 µL of DMSO with gently shaking. The absorbance of the solution was measured by Thermo Scientific Microplate Reader at 570 nm, and the relative cell viability was calculated according to the formula as follows:  $\text{viability (\%)} = (\text{Abs}_{570 \text{ sample}} - \text{Abs}_{570 \text{ control}}) / (\text{Abs}_{570 \text{ cell}} - \text{Abs}_{570 \text{ control}}) \times 100\%$ .

Two different cell lines: HepG2 and A549 cells were employed for assays of in vitro cytotoxicity of free PTX, the CHM blank and the PTX-loaded CHM. Typically, HepG2 (A549) cells were seeded in 96-well plates at the density of  $5 \times 10^3$  cells per well in 100 µL of corresponding complete medium (contains 90% DMEM/RPMI 1640 medium, 10% FBS, 100 units mL<sup>-1</sup> penicillin and 100 µg mL<sup>-1</sup> streptomycin), and then incubated in humidified incubator of 95% air and 5% CO<sub>2</sub> at 37 °C for 24 h. Subsequently, the medium was replaced by fresh corresponding medium containing serial dilutions of free PTX (5 and 10 µg mL<sup>-1</sup>; PTX was dissolved in DMSO and then diluted by cells culture media; the concentration of DMSO was less than 0.1%), the CHM blank and the PTX-loaded CHM (with the same PTX concentrations). All the experiments were conducted in duplicate with  $n = 6$  per sample. After incubation with cells for another 24 and 48 h, the cell viability was determined by MTT colorimetric assays.

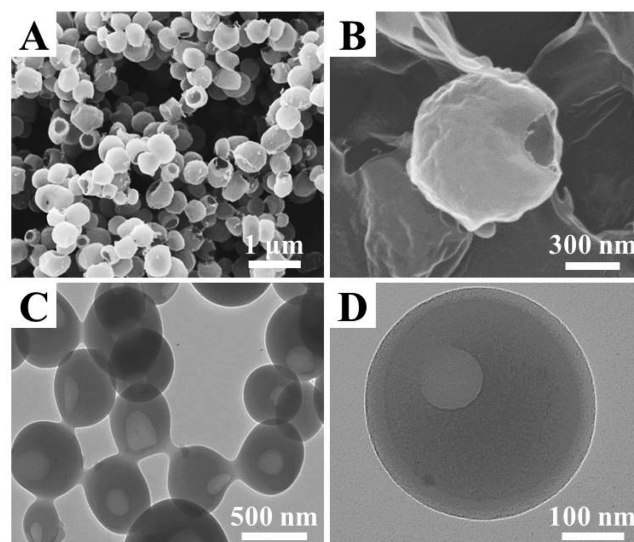
**2.7. Cell Uptake Analysis.** The real-time cellular uptake of the coumarin-6 loaded CHM were estimated on HepG2 cells by CLSM. In this study, HepG2 cells were first seeded in 24-well plate at the density of  $1 \times 10^5$  cells per well in cell culture medium and incubated with 10% FBS, 100 units mL<sup>-1</sup> penicillin and 100 µg mL<sup>-1</sup> streptomycin in humidified incubator of 95% air and 5% CO<sub>2</sub> at 37 °C for 12 h to allow cells attachment. Then, the cell culture was replaced with 1 mL fresh medium, containing free coumarin-6 (0.3 µg mL<sup>-1</sup>), BF (58 µg mL<sup>-1</sup>), GC (164 µg mL<sup>-1</sup>), coumarin-6 combined with BF or GC with same concentrations of BF or GC, the CHM blank (1.72 mg mL<sup>-1</sup>), and the coumarin-6 loaded CHM with same concentrations of coumarin-6, respectively. After incubation at 37 °C

for 12 h, the cells were washed three times with PBS (pH 7.4), then analyzed with a fluorescence microscope. The excitation wavelength value of coumarin-6 was 497 nm, while green fluorescence signals were observed at 532 nm. To explore the mechanism of internalization, real-time monitoring of cell uptake was carried out. HepG2 cells were seeded in a special CLSM cell culture dish with the same conditions. After 12 h of incubation, the cell culture was replaced with 1 mL fresh medium containing of the coumarin-6 loaded CHM (0.3 µg mL<sup>-1</sup> of coumarin-6), and monitored with the CLSM to obtain real-time fluorescence images and dynamic video immediately.

### 3. RESULTS AND DISCUSSIONS

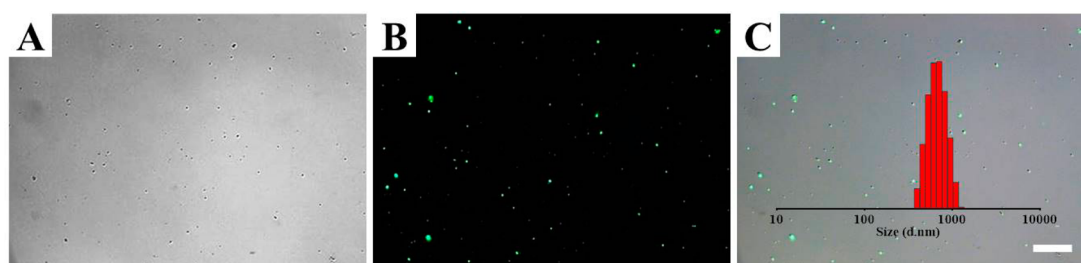
**3.1. Synthesis and Characterization of the CHM.** The CHM were fabricated by employing interfacial Schiff-base bonding reaction based on a dichloromethane/water emulsion (Scheme 1) of BF/GC. Different to the reported methods,<sup>19–24</sup> the CHM were prepared by utilizing hydrophobic BF small-molecules to fix macromolecules of hydrophilic GC at the O/W interface. The Schiff-base reaction does not create cross-linking structure as normal strategy.<sup>34,37,44–46</sup> It is the hydrophobic BF groups make an in situ precipitation of GC chains. Therefore, the resulted CHM could disperse in water very well owing to the exterior hydrophilic GC terminals. Meanwhile, its interior hydrophobic cavity is very suitable for loading lipophilic molecules or drugs.

Figure 1A shows the typical morphology of the obtained CHM. The spherical microstructure with an average size of 500



**Figure 1.** SEM (A, B) and TEM (C, D) images of the synthesized CHM.

nm was observed. The enlarged SEM image (Figure 1B) exposes the hollow microstructure with an opening, which may be caused by the treatment of removing organic solvent. Another reason might come from self-assembly process that usually create hollow microsphere with a hole.<sup>19,47,48</sup> In order to further confirm this phenomenon, TEM was used to check above features. Figure 1C reveals the typical CHM with the hole on each of those units. When zooming in to examine single one CHM (Figure 1D), we found the characteristic hole on the CHM. In addition, it has the distinct shell thickness of approximately 30 nm, which should be fabricated via the chemical bonds of Schiff base, thus demonstrating the interfacial Schiff-base bonding reaction a successful method on forming the CHM.



**Figure 2.** Characterization of the coumarin-6 loaded CHM: (A) the optical image; (B) the fluorescent image; and (C) the overlying image of A and B; inset is a result of DLS analysis. These microspheres have passed through a  $0.22\ \mu\text{m}$  filter membrane. The scale bar is  $25\ \mu\text{m}$ .

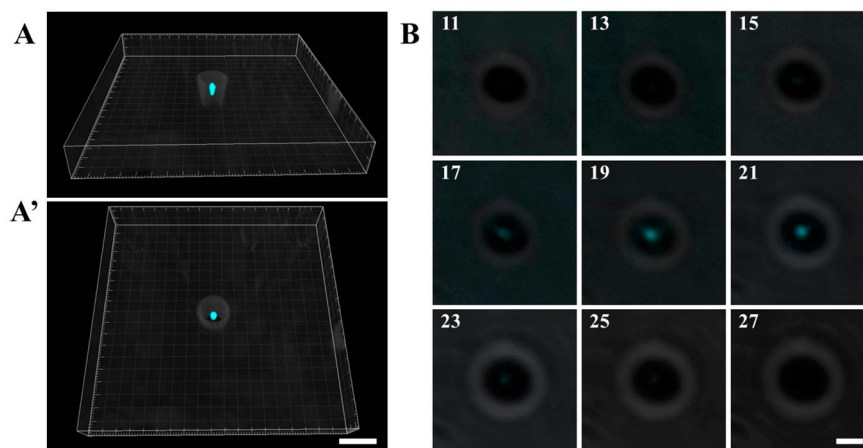


**Figure 3.** (A) 3D CLSM image of the Nile blue-loaded CHM. (B) The selected 2D pictures. The number on the picture denotes the layer sequence. The scale bar is (A)  $3\ \mu\text{m}$  and (B)  $1\ \mu\text{m}$ .

**3.2. Drug-Loading Capability of the CHM.** Coumarin-6 was first used as a model of lipophilic drug,<sup>49,50</sup> to study the loading capability of the formed microstructures. Figure 2A shows the optical image of the obtained microspheres. Their drug-loading capability was confirmed by the fluorescence microscopy (Figure 2B). After overlying these two images (Figure 2C), all the microspheres showed green fluorescence, demonstrating that coumarin-6 has been efficiently encapsulated in the microspheres. However, beyond our expectation, the size of these prepared microspheres displayed a relatively big and wide range of distribution, having an average size of  $400\text{--}1000\ \text{nm}$  (Figure 2C, inset) based on the measurement of DLS analysis. Although the size is agreeing with above SEM measurements (Figure 1), this result is not consistent with the theoretical size of below  $220\ \text{nm}$ , owing to the post-treatment of passing through the  $0.22\ \mu\text{m}$  apertures of filter paper (see section 2.3). As a supplementary data, the original microspheres showed a size distribution from  $100$  to  $2000\ \text{nm}$  (see Figure S5 and Table S1 in Supporting Information). We thus suspected that an adaptive transformation has been occurred in this CHM system.

Before discussing the adaptive transformation, a 3D CLSM examination was carried out to penetrate the Nile blue-loaded CHM (Nile-blue is used as the second model of lipophilic drug). In order to eliminate the solvent influence, the obtained microspheres were treated with a vacuum freeze-dry technology. Then, they were redispersed in deionized water for the measurement. Figure 3A,A' shows the 3D feature of the dye-loaded CHM. The lighted microsphere confirmed that the Nile blue was successfully entrapped in the CHM. Then, we drew out the 2D layers (Figure 3B, total 29 layers) separately,

checking the orientational distribution of dye molecules. We found that dye molecules got together in the core (Figure 3B, from 11 to 27) rather than our previously expected around the inner shell. This aggregation might come into being within the drying treatment and confinement of GC chains. Nevertheless, this insight not only proved the drug-loading capability but also revealed the loading pattern within the CHM. Furthermore, the quantitative studies showed that this kind CHM displayed a high loading ability with a DLE of  $37.5 \pm 5.0\%$  and a DEE of  $75.0 \pm 3.0\%$  for the PTX, based on the standard curve as shown in Figure S6.

**3.3. Shape-Adaptive Transformation of the CHM.** We obtained above-mentioned CHM after passing through the  $0.22\ \mu\text{m}$  microporous membrane, which is a sterile pretreatment for cell culture.<sup>51,52</sup> Considering that numerous BF molecules (having single bonding site beside the hydrophobic group) held GC polymers, this microstructure might be somewhat soft and flexible. We thus supposed that the CHM might go through a smaller channel less than the size of itself (Figure 4A), illustrating a shape-adaptive ability. On the basis of this hypothesis, we carried out SEM measurements on the cross-section of the employed microporous membrane before and after the usage. Figure 4B shows the whole cross-section of the membrane, where a gradient porous structure is exhibited. Fine pores with a standard of  $0.22\ \mu\text{m}$  are loaded on the up layer, while the base layer is large openings that act as supporting basement. When zooming in to observe the microstructure of the up layer, porous scaffold structure (Figure 4C) is exhibited. After careful checking the used membrane, shape-adaptive changing of the CHM could be observed (Figures 4D and S7). Figure 4D<sub>1</sub> and D<sub>2</sub> display a distinct radial shrinkage of the

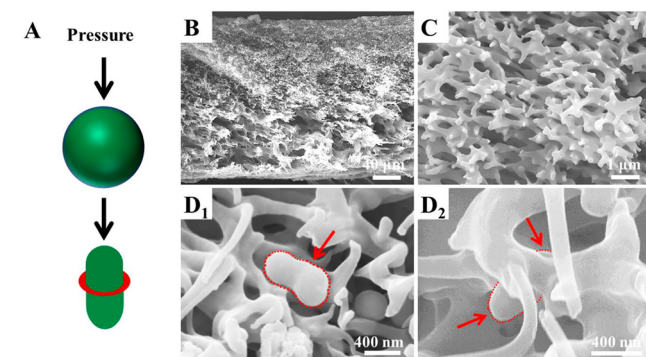


**Figure 4.** (A) Schematic illustration of the shape-adaptive property of the CHM. (B, C) Sectional view of the filter membrane ( $0.22\ \mu\text{m}$ ), and (D) the shape-adaptive transformation of the CHM when passing through the microporous membrane. Red arrows denote the transformed CHM.

passing through CHM in situ, which demonstrated our hypothesis for the shape-adaptive capability of the CHM. The shape changing is happened from circular microspheres to elliptical microspheres, which may endow the CHM with preferential cellular uptake, larger contact surface area, higher targeting ability, and accumulation at the target site compared to spheres.<sup>53–55</sup>

**3.4. pH-Responsive Behavior of the CHM.** Schiff-base is known unstable in acidic condition. The acid-triggered decomposition of the CHM was estimated in the pH range from 7.06 to 5.01. Figure S8 represents the pH-responsive behaviors of the prepared CHM. In neutral (pH 7.06) and slight acidic medium (pH 6.03), the morphology of microspheres did not change whether in the initial phase (Figure S8A,B) or after 10 min treatment (Figure S8A',B'). When the pH value was 5.01, microspheres swelled first (Figure S8C) and then started to decompose after 10 min (Figure S8C').

In order to further confirm the stability of the prepared CHM under different pH, a series of cryo-SEM measurements (Figure 5) were carried out for a prolonged period of time (2

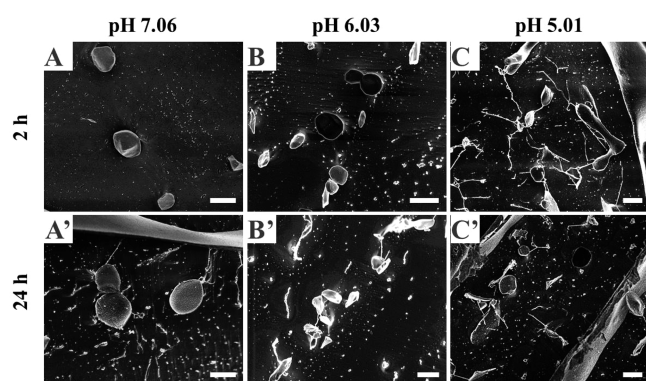


**Figure 5.** Cryo-SEM images of the CHM in various pH mediums after 2 h (A, B, and C) and 24 h (A', B', and C') treatments: A, A': pH 7.06; B, B': pH 6.03; C, C': pH 5.01. All scale bars are  $1\ \mu\text{m}$ .

and 24 h). In neutral condition (pH 7.06), the morphology of CHM did not change even after 24 h treatment (Figure 5A'). This result is in agreement with the stability of some reported Schiff-base microstructures.<sup>56,57</sup> But in slight acidic medium (pH 6.03), slight shrinkage was found when the treatment was prolonged from 2 h (Figure 5B) to 24 h (Figure 5B'). When

pH 5.01 was employed, most of microspheres had decomposed just after 2 h treatment (Figure 5C) due to hydrolysis of the Schiff base bond. All these results demonstrated that the CHM were relatively stable within neutral or weak-acid conditions, compared with the reported Schiff-base system.<sup>44,58,59</sup> In our viewpoint, this phenomenon is owing to the bonding of those big hydrophobic BF groups on the GC chains. The changing wettability may limit the permeation of acidic solution, thus making main contribution for their stability and above responsiveness.

**3.5. In Vitro PTX Release.** The in vitro releasing capability of PTX-loaded CHM in different pH medium was assessed by a common-used dialysis procedure.<sup>60</sup> The accumulated percentages of PTX released from PTX-loaded CHM in 48 h were studied in PBS solutions with pH 7.06, 6.03, or 5.01 (Figure 6).

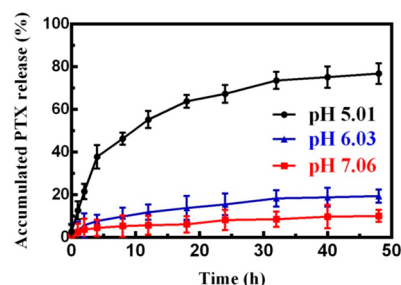


**Figure 6.** In vitro drug release of PTX-loaded CHM in PBS at pH 7.06 (red solid), 6.03 (blue triangle), and 5.01 (black dot) at  $37\ ^\circ\text{C}$  ( $n = 3$  for each pH value).

In simulated physiological conditions (pH 7.06, red solid) and slight acidic conditions (pH 6.03, blue triangle), the cumulative release amounts of PTX were  $10.0 \pm 2.8\%$  and  $19.3 \pm 3.0\%$  over 48 h from PTX-CHM, respectively. While PTX cumulative release amount was significantly increased to approximately  $76.8 \pm 4.8\%$  at pH 5.01 (black dot), going with a fast release rate. These results consistent with above-mentioned images (Figures 5 and S7). The cleavage of Schiff base linkage between GC and BF plays the crucial rule, which can be accelerated at lower pH condition.<sup>61,62</sup>

**3.6. Efficacy of the PTX-Loaded CHM as Drug Carrier.** In evaluating efficacy of the PTX-loaded CHM, MTT colorimetric assay is known as a general method.<sup>41</sup> Cellular cytotoxicity or biocompatibility of the CHM carrier can be also evaluated. The BF, GC and the CHM blank exhibited little cytotoxicity to L929 cells at different concentrations even after 48 h of incubation (Figure S9). It demonstrated that the microspheres have excellent biocompatibility.

In evaluating efficacy of the CHM carrier, PTX was loaded in the CHM and used as a basic drug model on two typical cell lines: HepG2 and A549 cells. First, MTT assays showed that free PTX exhibited detectable cytotoxicity on both HepG2 and A549 cells at the tested PTX concentrations of 5 and  $10\ \mu\text{g mL}^{-1}$  (Figure 7A). They all displayed an increasing cytotoxicity with the increase of PTX concentration and the prolongation of incubation time. It is consistent with previous reports.<sup>63,64</sup> Then, we observed that the blank CHM were practically safe (cell viability  $> 95\%$ ) on HepG2 and A549 cells after 24 h incubation at the denoted CHM concentrations of  $0.86$  and  $1.72\ \text{mg mL}^{-1}$  (Figure 7B), respectively, meaning that the CHM is a more biocompatible carrier than plain chitosan.<sup>65,66</sup> HepG2 cells were more sensitive to the CHM than A549 cells, since cell viability on HepG2 rather than A549 decreased clearly after 48

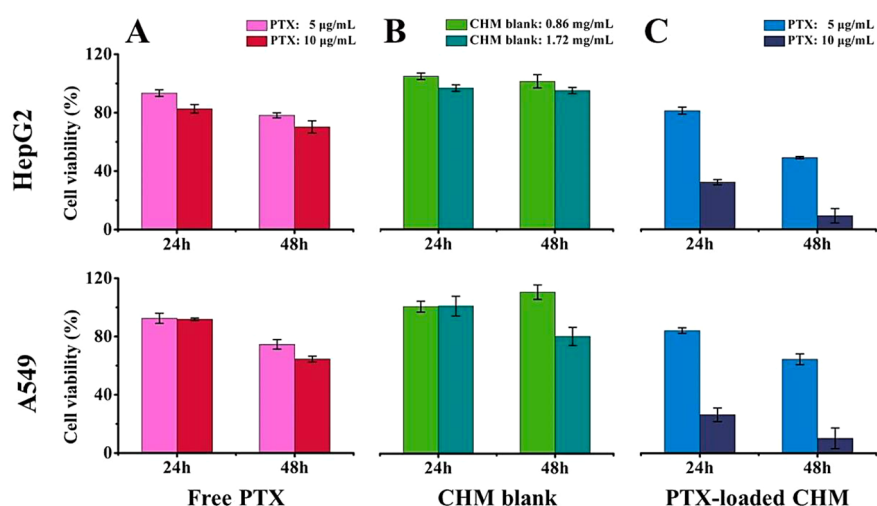


**Figure 7.** MTT assays of (A) free PTX, (B) the CHM blank, and (C) the PTX-loaded CHM on HepG2 and A549 cells at denoted times. The control (no treated cells) was taken as 100%. The data are presented as the mean plus or minus the standard deviation ( $n = 6$  for each group).

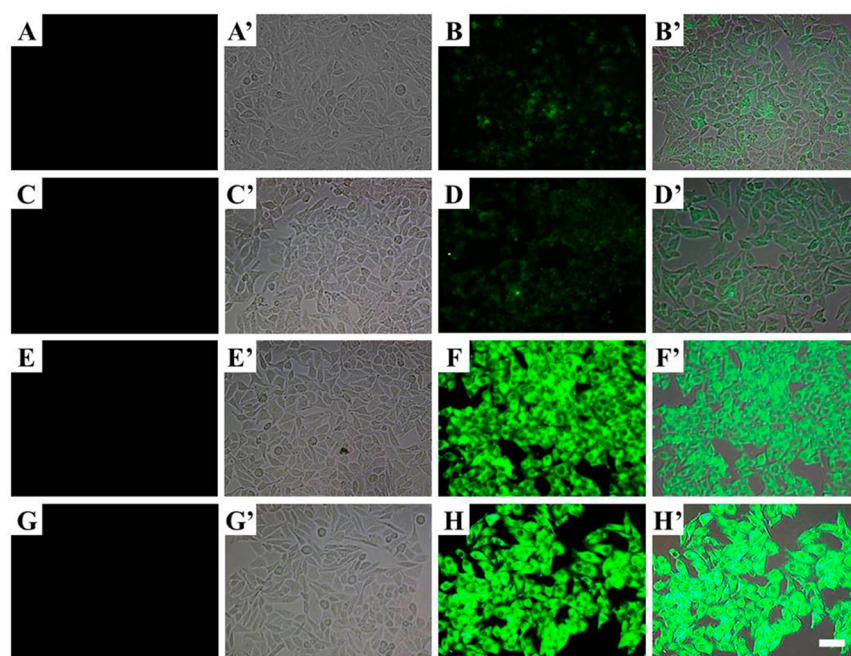


**Figure 8.** In vitro evaluation of cellular uptake under different dose conditions. (A, A') blank; (B, B') coumarin-6; (C, C') BF; (D, D') coumarin-6 combined with BF; (E, E') GC; (F, F') coumarin-6 combined with GC; (G, G') the blank CHM; (H, H') the coumarin-6 loaded CHM; (A–H) fluorescent images; (A'–H') overlaying of fluorescent and optical images. The scale bar is 25  $\mu\text{m}$ .

h incubation at the higher concentration. According to the MTT results, we employed the CHM concentration of 0.86  $\text{mg mL}^{-1}$  for efficacy testing of this carrier. When PTX concentration was 5  $\mu\text{g mL}^{-1}$ , viabilities of the two cells treated with the PTX-loaded CHM appeared some decrease at initial 24 h (Figure 7C, light blue). This maybe depended on the effective concentration of PTX itself.<sup>63</sup> Significantly, when PTX concentration was 10  $\mu\text{g mL}^{-1}$ , the PTX-loaded CHM showed distinct cytotoxicity (Figure 7C, dark blue) compared with free PTX in spite of using the same drug concentrations. This improvement ( $t$  test,  $P < 0.05$ , also see Table S2 for data details) can be attributed to the efficient load and release of PTX molecules from the CHM carriers. It was further proved by the prolongation of incubation time (Figure 7C, 48 h).

**3.7. Cell Uptake Analysis.** This synthesized CHM was demonstrated to be a good drug carrier because of its advances, such as hydrophilic chitosan surface, enough interior for hydrophobic drugs, suitable size, shape-adaptive character, and pH responsiveness. Although the chitosan surface is well-known for its cell affinity, the novel design of this CHM still makes it a smart drug carrier. For detecting the mechanism details, the cellular uptake of coumarin-6 loaded CHM was analyzed qualitatively on HepG2 cells by using fluorescence microscope. HepG2 cells were incubated with different coumarin-6 formulations including plain coumarin-6 and coumarin-6 combined with GC, BF, and the CHM, respectively. Figure 8 shows the intuitive display of the results directly. All test groups (Figure 8A–H) present the normal cells morphology (Figure 8A), indicating good metabolism of

all studied cells under test conditions. Cells incubated with plain coumarin-6 (Figure 8B) or coumarin-6 combined with BF (Figure 8D) showed the same slight fluorescence signal, respectively. These phenomena proved that small hydrophobic molecules usually played less effect on cell uptake. However, coumarin-6 combined with GC group (Figure 8F) exhibited a higher intracellular fluorescence density, because GC could carry hydrophobic dyes into cells.<sup>67,68</sup> But, we carried out the MTT assays on both HepG2 and A549 cells using free PTX mixed with GC, the results did not support plain GC a valuable drug carrier for PTX (Figure S8 in Supporting Information). When HepG2 cells were incubated with the coumarin-6 loaded CHM (Figure 8H), the green fluorescence signal was more intense than the plain GC group. This fluorescence was not caused by dyes adhered on the surface of the cell membranes because any dissociative CHM or free coumarin-6 have been washed off with PBS. Meanwhile, we did not find that the dimension of the prepared CHM (400–1000 nm, Figure 2C, inset) had negative influence for cell uptake maybe due to its shape-adaptive property.<sup>9,69</sup> Combined with aforementioned MTT assays, these recorded images well supported the high efficacy of the CHM carrier.

In order to observe the mode of internalization, real-time fluorescence detection was performed on this carrier system. Figure 9A shows an observation that one HepG2 cell is

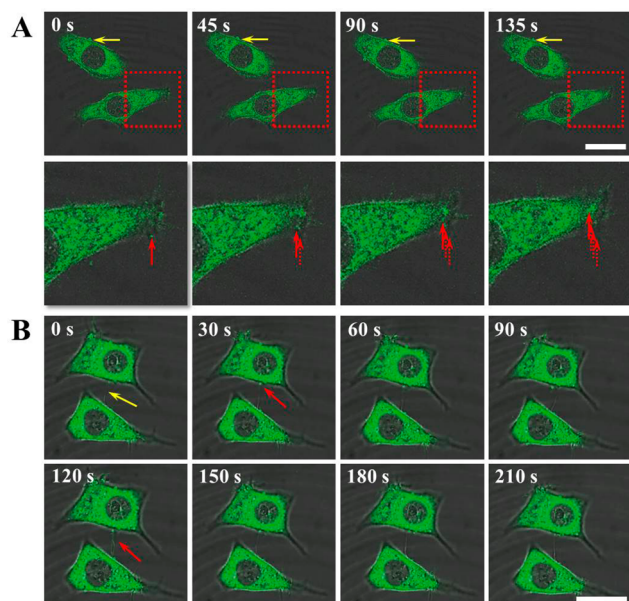


**Figure 9.** (A) HepG2 cells uptake the coumarin-6 loaded CHM within 3 min; (B) the fast release of the coumarin-6 loaded CHM in HepG2 cells within 3 min. The scale bar is 25  $\mu\text{m}$ .

engulfing the coumarin-6 loaded CHM within 3 min (based on a video of details that was recorded after 2 h coincubation with coumarin-6 loaded CHM). The fluorescent CHM were engulfed quickly and distinctly through the cell's protrusions (red arrow) rather than cell's body (yellow arrow). Unlike previous report that the internalization of cationic chitosan microspheres appears to occur predominantly by adsorptive endocytosis,<sup>70</sup> this uptake process is more like a phagocytosis that can be simply called cell eating. Anyway, the CHM were enclosed from extracellular environment with high efficiency.

Furthermore, we luckily recorded a group of images (Figure 9B) that demonstrated the fast response of the CHM on entry

into a cell. Figure 9B, 0 s shows two HepG2 cells that are connected with one filopodia (yellow arrow). After 30 s, a coumarin-6 loaded CHM (red arrow) was found near the base of the filopodia. Then, just in the next 90 s, the image (Figure 9B, 120 s) recorded that the filopodia was lightened with green fluorescence (red arrows). And immediately, the lightened green disappeared on the filopodia in situ within no more than 30 s (Figure 9B, 150 s). We thus speculated that this sudden flash could be attributed to the fast release of the loaded fluorescent molecules. In other words, it is reasonable to make the judgment that the novel Schiff-base constructed CHM just undergo a complete process from cargo carrying to entering the cell and then to releasing coumarin-6 with in totally 90 s. These phenomena not only let us know that the CHM is easy to enter into cells but also show us its fast responsiveness in cells in situ.

#### 4. CONCLUSION

In summary, we have designed and successfully prepared the CHM as a new carrier for tough hydrophobic drugs. The interfacial Schiff-base bonding between hydrophobic BF molecules and biocompatible GC polymers is highlighted due to it making the resulted microstructure a promising drug carrier manner with smart capabilities and high efficiency. Especially, its shape-adaptive and pH-responsive features play the crucial rule in the whole process from fabrication to utilization. The former makes the drug loading stable and dilatation; the latter ensures the drug releasing fast and efficient. In vitro cellular uptake analyses displayed for the first time the real-time phagocytosis of the CHM and the in situ intracellular release of the loaded fluorescent molecules. MTT assays further demonstrated good efficacy of the PTX-loaded CHM. Considering that shape adaptability may offer new opportunities in controlling long-circulation and transport across biobarriers, the CHM carrier is prospective in controlled drug delivery particularly. This work is now under investigation. The deeper understanding of the phagocytosis mechanism is also expected. Since this unique assembly strategy supplies advantages such as facile fabrication, low cost but high efficiency to form intelligent drug carrier, we believe this CHM model would open a new avenue for tough drugs on treating tumors.

#### ■ ASSOCIATED CONTENT

##### Supporting Information

The Supporting Information is available free of charge on the ACS Publications website at DOI: 10.1021/acs.biomac.7b00592.

Synthesis of BF, FT-IR, <sup>1</sup>H NMR, GC-MS, DLS, pH-responsive behaviors (optical microscope), morphologies of the shape adaptive CHM, MTT on L929, and MTT data details (PDF).

#### ■ AUTHOR INFORMATION

##### Corresponding Author

\*E-mail: wangxing@mail.buct.edu.cn.

##### ORCID

Lei Tao: 0000-0002-1735-6586

Xing Wang: 0000-0002-9990-1479

### Author Contributions

The manuscript was written through contributions of all authors. All authors have given approval to the final version of the manuscript.

### Funding

National Natural Science Foundation of China (21574008) and the Fundamental Research Funds for Central Universities (PYBZ1709, XK1701) are used to support the research.

### Notes

The authors declare no competing financial interest.

### ACKNOWLEDGMENTS

The authors thank the National Natural Science Foundation of China (21574008) and the Fundamental Research Funds for Central Universities (PYBZ1709, XK1701) of China for their financial support.

### ABBREVIATIONS

GC, glycol chitosan; CH<sub>2</sub>Cl<sub>2</sub>, dichloromethane; DCC, *N,N*-dicyclohexylcarbodiimide; DMAP, 4-(dimethylamino) pyridine; PTX, paclitaxel; MTT, 3-(4,5-dimethylazolyl-2)-2,5-diphenyl tetrazolium bromide; THF, tetrahydrofuran; BF, borneol 4-formylbenzoate; CHM, chitosan hollow microspheres; L929, the mouse fibroblast cells; HepG2, the human hepatocarcinoma cells; A549, human nonsmall lung cancer cells; DMEM, Dulbecco's modified Eagle's medium; RPMI 1640, Roswell Park Memorial Institute 1640 medium; FBS, fetal bovine serum; SEM, scanning electron microscopy; TEM, transmission electron microscope; DLS, dynamic light scattering; CLSM, confocal laser scanning microscopy; DLE, drug loading efficiency; DEE, drug encapsulation efficiency; cryo-SEM, cryo-scanning electron microscope

### REFERENCES

- (1) Yue, Z. G.; Wei, W.; You, Z. X.; Yang, Q. Z.; Yue, H.; Su, Z. G.; Ma, G. H. Iron Oxide Nanotubes for Magnetically Guided Delivery and pH-Activated Release of Insoluble Anticancer Drugs. *Adv. Funct. Mater.* **2011**, *21*, 3446–3453.
- (2) Guo, Y. Y.; Chu, M.; Tan, S. W.; Zhao, S.; Liu, H. X.; Otieno, B. O.; Yang, X. L.; Xu, C. R.; Zhang, Z. P. Chitosan-g-TPGS Nanoparticles for Anticancer Drug Delivery and Overcoming Multidrug Resistance. *Mol. Pharmacol.* **2014**, *11*, 59–70.
- (3) Stuurman, F. E.; Nuijen, B.; Beijnen, J. H.; Schellens, J. H. M. Oral Anticancer Drugs: Mechanisms of Low Bioavailability and Strategies for Improvement. *Clin. Pharmacokinet.* **2013**, *52*, 399–414.
- (4) Tiwari, G.; Tiwari, R.; Sriwastawa, B.; Bhati, L.; Pandey, S.; Pandey, P.; Bannerjee, S. K. Drug Delivery Systems: an Updated Review. *Int. J. Pharm. Invest.* **2012**, *2* (1), 2–11.
- (5) Kozlovskaya, V.; Xue, B.; Kharlampieva, E. Shape-Adaptable Polymeric Particles for Controlled Delivery. *Macromolecules* **2016**, *49*, 8373–8386.
- (6) Yan, Z. Q.; Wang, F.; Wen, Z. Y.; Zhan, C. Y.; Feng, L. L.; Liu, Y.; Wei, X. L.; Xie, C.; Lu, W. Y. LyP-1-Conjugated PEGylated Liposomes: a Carrier System for Targeted Therapy of Lymphatic Metastatic Tumor. *J. Controlled Release* **2012**, *157*, 118–125.
- (7) Yu, H. J.; Cui, Z. R.; Yu, P. C.; Guo, C. Y.; Feng, B.; Jiang, T. Y.; Wang, S. L.; Yin, Q.; Zhong, D. F.; Yang, X. L.; Zhang, Z. W.; Li, Y. P. pH- and NIR Light-Responsive Micelles with Hyperthermia Triggered Tumor Penetration and Cytoplasm Drug Release to Reverse Doxorubicin Resistance in Breast Cancer. *Adv. Funct. Mater.* **2015**, *25*, 2489–2500.
- (8) Cai, B.; Zhao, M. G.; Ma, Y.; Ye, Z. Z.; Huang, J. Y. Bioinspired Formation of 3D Hierarchical CoFe<sub>2</sub>O<sub>4</sub> Porous Microspheres for Magnetic-Controlled Drug Release. *ACS Appl. Mater. Interfaces* **2015**, *7*, 1327–1333.

- (9) Chen, J.; Kozlovskaya, V.; Goins, A.; Campos-Gomez, J.; Saeed, M.; Kharlampieva, E. Biocompatible Shaped Particles from Dried Multilayer Polymer Capsules. *Biomacromolecules* **2013**, *14*, 3830–3841.

- (10) Deguchi, S.; Ifuku, N. Bottom-Up Formation of Dodecane-in-Water Nanoemulsions from Hydrothermal Homogeneous Solutions. *Angew. Chem., Int. Ed.* **2013**, *52*, 6409–6412.

- (11) Han, L.; Tang, C.; Yin, C. H. pH-Responsive Core-Shell Structured Nanoparticles for Triple-Stage Targeted Delivery of Doxorubicin to Tumors. *ACS Appl. Mater. Interfaces* **2016**, *8*, 23498–23508.

- (12) Barner, L. Synthesis of Microspheres as Versatile Functional Scaffolds for Materials Science Applications. *Adv. Mater.* **2009**, *21*, 2547–2553.

- (13) Berkland, C.; Kim, K.; Pack, D. W. Fabrication of PLG Microspheres with Precisely Controlled and Monodisperse Size Distributions. *J. Controlled Release* **2001**, *73*, 59–74.

- (14) Sun, L. L.; Li, Y. H.; Yang, P.; Zhu, G. J.; Dovichi, N. J. High Efficiency and Quantitatively Reproducible Protein Digestion by Trypsin-Immobilized Magnetic Microspheres. *J. Chromatogr. A* **2012**, *1220*, 68–74.

- (15) Ahsan, F.; Rivas, I. P.; Khan, M. A.; Suárez, A. I. T. Targeting to Macrophages: Role of Physicochemical Properties of Particulate Carriers-Liposomes and Microspheres-on the Phagocytosis by Macrophages. *J. Controlled Release* **2002**, *79*, 29–40.

- (16) Freiberg, S.; Zhu, X. X. Polymer Microspheres for Controlled Drug Release. *Int. J. Pharm.* **2004**, *282*, 1–18.

- (17) Lynn, D. M.; Amiji, M. M.; Langer, R. pH-Responsive Polymer Microspheres: Rapid Release of Encapsulated Material within the Range of Intracellular pH. *Angew. Chem., Int. Ed.* **2001**, *40*, 1707–1710.

- (18) Lu, C. Y.; Mu, B.; Liu, P. Stimuli-Responsive Multilayer Chitosan Hollow Microspheres via Layer-by-Layer Assembly. *Colloids Surf., B* **2011**, *83*, 254–259.

- (19) Sun, Q. H.; Deng, Y. L. In Situ Synthesis of Temperature-Sensitive Hollow Microspheres via Interfacial Polymerization. *J. Am. Chem. Soc.* **2005**, *127*, 8274–8275.

- (20) Li, J.; Jiang, H. K.; Ouyang, X.; Han, S. H.; Wang, J.; Xie, R.; Zhu, W. T.; Ma, N.; Wei, H.; Jiang, Z. Y. CaCO<sub>3</sub>/Tetraethylenepentamine-Graphene Hollow Microspheres as Biocompatible Bone Drug Carriers for Controlled Release. *ACS Appl. Mater. Interfaces* **2016**, *8*, 30027–30036.

- (21) Toprak, M. S.; McKenna, B. J.; Mikhaylova, M.; Waite, J. H.; Stucky, G. D. Spontaneous Assembly of Magnetic Microspheres. *Adv. Mater.* **2007**, *19*, 1362–1368.

- (22) Hanley, C. A.; McCarthy, J. E.; Purcell-Milton, F.; Gerard, V.; McCloskey, D.; Donegan, J.; Rakovich, Y. P.; Gun'ko, Y. K. Preparation and Investigation of Quantum-Dot-Loaded Hollow Polymer Microspheres. *J. Phys. Chem. C* **2013**, *117*, 24527–24536.
- (23) Wang, J. Z.; Loh, K. P.; Zhong, Y. L.; Lin, M.; Ding, J.; Foo, Y. L. Bifunctional FePt Core-Shell and Hollow Spheres: Sonochemical Preparation and Self-Assembly. *Chem. Mater.* **2007**, *19*, 2566–2572.

- (24) Du, P. C.; Zeng, J.; Mu, B.; Liu, P. Biocompatible Magnetic and Molecular Dual-Targeting Polyelectrolyte Hybrid Hollow Microspheres for Controlled Drug Release. *Mol. Pharmaceutics* **2013**, *10*, 1705–1715.

- (25) Kumar, M. N. V. R.; Muzzarelli, R. A. A.; Muzzarelli, C.; Sashiwa, H.; Domb, A. J. Chitosan Chemistry and Pharmaceutical Perspectives. *Chem. Rev.* **2004**, *104*, 6017–6084.

- (26) İkinci, G.; Şenel, S.; Akıncıbay, H.; Kaş, S.; Erciç, S.; Wilson, C. G.; Hincal, A. A. Effect of Chitosan on a Periodontal Pathogen *Porphyromonas gingivalis*. *Int. J. Pharm.* **2002**, *235*, 121–127.

- (27) Sung, H. W.; Sonaje, K.; Liao, Z. X.; Hsu, L. W.; Chuang, E. Y. pH-Responsive Nanoparticles Shelled with Chitosan for Oral Delivery of Insulin: From Mechanism to Therapeutic Applications. *Acc. Chem. Res.* **2012**, *45* (4), 619–629.

- (28) Peng, S. F.; Yang, M. J.; Su, C. J.; Chen, H. L.; Lee, P. W.; Wei, M. C.; Sung, H. W. Effects of Incorporation of Poly( $\gamma$ -Glutamic Acid)

in Chitosan/DNA Complex Nanoparticles on Cellular Uptake and Transfection Efficiency. *Biomaterials* **2009**, *30*, 1797–1808.

(29) Ye, Y. Q.; Yang, F. L.; Hu, F. Q.; Du, Y. Z.; Yuan, H.; Yu, H. Y. Core-Modified Chitosan-Based Polymeric Micelles for Controlled Release of Doxorubicin. *Int. J. Pharm.* **2008**, *352*, 294–301.

(30) Hu, H. B.; Yu, L.; Tan, S. W.; Tu, K. H.; Wang, L. Q. Novel Complex Hydrogels Based on N-Carboxyethyl Chitosan and Quaternized Chitosan and Their Controlled in Vitro Protein Release Property. *Carbohydr. Res.* **2010**, *345*, 462–468.

(31) Thanou, M.; Verhoef, J. C.; Junginger, H. E. Oral Drug Absorption Enhancement by Chitosan and Its Derivatives. *Adv. Drug Delivery Rev.* **2001**, *52*, 117–126.

(32) Thanou, M. M.; Kotzé, A. F.; Scharringhausen, T.; Lueßen, H. L.; de Boer, A. G.; Verhoef, J. C.; Junginger, H. E. Effect of Degree of Quaternization of N-Trimethyl Chitosan Chloride for Enhanced Transport of Hydrophilic Compounds across Intestinal Caco-2 Cell Monolayers. *J. Controlled Release* **2000**, *64*, 15–25.

(33) Lepeltier, E.; Loretz, B.; Desmaële, D.; Zapp, J.; Herrmann, J.; Couvreur, P.; Lehr, C. M. Squalenoylation of Chitosan: A Platform for Drug Delivery? *Biomacromolecules* **2015**, *16*, 2930–2939.

(34) Liu, L.; Yang, J. P.; Ju, X. J.; Xie, R.; Liu, Y. W.; Wang, W.; Zhang, J. J.; Niu, C. H.; Chu, L. Y. Monodisperse Core-Shell Chitosan Microspheres for pH-Responsive Burst Release of Hydrophobic Drugs. *Soft Matter* **2011**, *7*, 4821–4827.

(35) Zhang, Y. L.; Tao, L.; Li, S. X.; Wei, Y. Synthesis of Multiresponsive and Dynamic Chitosan-Based Hydrogels for Controlled Release of Bioactive Molecules. *Biomacromolecules* **2011**, *12*, 2894–2901.

(36) Yang, B.; Zhang, Y. L.; Zhang, X. Y.; Tao, L.; Li, S. X.; Wei, Y. Facilely Prepared Inexpensive and Biocompatible Self-Healing Hydrogel: a New Injectable Cell Therapy Carrier. *Polym. Chem.* **2012**, *3*, 3235–3238.

(37) Jia, T.; Huang, S.; Yang, C. J.; Wang, M. F. Unimolecular Micelles of Amphiphilic Cyclodextrin-Core Star-Like Copolymers with Covalent pH-Responsive Linkage of Anticancer Prodrugs. *Mol. Pharmaceutics* **2016**, DOI: 10.1021/acs.molpharmaceut.6b00708.

(38) Rinaudo, M. Chitin and Chitosan: Properties and Applications. *Prog. Polym. Sci.* **2006**, *31*, 603–632.

(39) Yang, H.; Xun, Y.; Li, Z.; Hang, T.; Zhang, X.; Cui, H. Influence of Borneol on in Vitro Corneal Permeability and on in Vivo and in Vitro Corneal Toxicity. *J. Int. Med. Res.* **2009**, *37*, 791–802.

(40) Dai, J. P.; Chen, J.; Bei, Y. F.; Han, B. X.; Wang, S. Influence of Borneol on Primary Mice Oral Fibroblasts: a Penetration Enhancer may be Used in Oral Submucous Fibrosis. *J. Oral Pathol. Med.* **2009**, *38*, 276–281.

(41) Lv, P. P.; Wei, W.; Yue, H.; Yang, T. Y.; Wang, L. Y.; Ma, G. H. Porous Quaternized Chitosan Nanoparticles Containing Paclitaxel Nanocrystals Improved Therapeutic Efficacy in Non-Small-Cell Lung Cancer after Oral Administration. *Biomacromolecules* **2011**, *12*, 4230–4239.

(42) Amoozgar, Z.; Park, J.; Lin, Q. N.; Yeo, Y. Low Molecular-Weight Chitosan as a pH-Sensitive Stealth Coating for Tumor-Specific Drug Delivery. *Mol. Pharmaceutics* **2012**, *9*, 1262–1270.

(43) Lu, L.; Unsworth, L. D. pH-Triggered Release of Hydrophobic Molecules from Self-Assembling Hybrid Nanoscaffolds. *Biomacromolecules* **2016**, *17*, 1425–1436.

(44) Wei, W.; Yuan, L.; Hu, G.; Wang, L. Y.; Wu, J.; Hu, X.; Su, Z. G.; Ma, G. H. Monodisperse Chitosan Microspheres with Interesting Structures for Protein Drug Delivery. *Adv. Mater.* **2008**, *20*, 2292–2296.

(45) Wei, J.; Ju, X. J.; Zou, X. Y.; Xie, R.; Wang, W.; Liu, Y. M.; Chu, L. Y. Multi-Stimuli-Responsive Microcapsules for Adjustable Controlled-Release. *Adv. Funct. Mater.* **2014**, *24*, 3312–3323.

(46) Zhang, H. Y.; Yong, X. Y.; Zhou, J. Y.; Deng, J. P.; Wu, Y. P. Biomass Vanillin-Derived Polymeric Microspheres Containing Functional Aldehyde Groups: Preparation, Characterization, and Application as Adsorbent. *ACS Appl. Mater. Interfaces* **2016**, *8*, 2753–2763.

(47) Wang, X.; Liu, N.; Yan, X.; Zhang, W. J.; Wei, Y. Alkali-Guided Synthesis of Polyaniline Hollow Microspheres. *Chem. Lett.* **2005**, *34*, 42–43.

(48) Bai, M. Y.; Cheng, Y. J.; Wickline, S. A.; Xia, Y. N. Colloidal Hollow Spheres of Conducting Polymers with Smooth Surface and Uniform, Controllable Sizes. *Small* **2009**, *5*, 1747–1752.

(49) Lu, W.; Zhang, Y.; Tan, Y. Z.; Hu, K. L.; Jiang, X. G.; Fu, S. K. Cationic Albumin-Conjugated Pegylated Nanoparticles as Novel Drug Carrier for Brain Delivery. *J. Controlled Release* **2005**, *107*, 428–448.

(50) Pretor, S.; Bartels, J.; Lorenz, T.; Dahl, K.; Finke, J. H.; Peterat, G.; Krull, R.; Al-Halhouli, A. T.; Dietzel, A.; Büttgenbach, S.; Behrends, S.; Reichl, S.; Müller-Goymann, C. C. Cellular Uptake of Coumarin-6 under Microfluidic Conditions into HCE-T Cells from Nanoscale Formulations. *Mol. Pharmaceutics* **2015**, *12*, 34–45.

(51) Madaeni, S. S. The Application of Membrane Technology for Water Disinfection. *Water Res.* **1999**, *33*, 301–308.

(52) Wang, Y. Y.; Hammes, F.; Düggelin, M.; Egli, T. Influence of Size, Shape, and Flexibility on Bacterial Passage through Micropore Membrane Filters. *Environ. Sci. Technol.* **2008**, *42*, 6749–6754.

(53) Gratton, S. E. A.; Ropp, P. A.; Pohlhaus, P. D.; Luft, J. C.; Madden, V. J.; Napier, M. E.; DeSimone, J. M. The Effect of Particle Design on Cellular Internalization Pathways. *Proc. Natl. Acad. Sci. U. S. A.* **2008**, *105*, 11613–11618.

(54) Sharma, G.; Valenta, D. T.; Altman, Y.; Harvey, S.; Xie, H.; Mitragotri, S.; Smith, J. W. Polymer Particle Shape Independently Influences Binding and Internalization by Macrophages. *J. Controlled Release* **2010**, *147*, 408–412.

(55) Muro, S.; Garnacho, G.; Champion, J. A.; Lefevovich, J.; Gajewski, C.; Schuchman, E. H.; Mitragotri, S.; Muzykantov, V. R. Control of Endothelial Targeting and Intracellular Delivery of Therapeutic Enzymes by Modulating the Size and Shape of ICAM-1-targeted Carriers. *Mol. Ther.* **2008**, *16* (8), 1450–1458.

(56) Ke, X. Y.; Coady, D. J.; Yang, C.; Engler, A. C.; Hedrick, J. L.; Yang, Y. Y. pH-Sensitive Polycarbonate Micelles for Enhanced Intracellular Release of Anticancer Drugs: a Strategy to Circumvent Multidrug Resistance. *Polym. Chem.* **2014**, *5*, 2621–2628.

(57) Yu, Y.; Chen, C. K.; Law, W. C.; Sun, H. T.; Prasad, P. N.; Cheng, C. A Degradable Brush Polymer-Drug Conjugate for pH-Responsive Release of Doxorubicin. *Polym. Chem.* **2015**, *6*, 953–961.

(58) Huang, W.; Wang, Y. J.; Zhang, S.; Huang, L.; Hua, D. B.; Zhu, X. L. A Facile Approach for Controlled Modification of Chitosan under  $\gamma$ -Ray Irradiation for Drug Delivery. *Macromolecules* **2013**, *46*, 814–818.

(59) Wang, X.; Yang, Y. Y.; Zhuang, Y. P.; Gao, P. Y.; Yang, F.; Shen, H.; Guo, H. X.; Wu, D. C. Fabrication of pH-Responsive Nanoparticles with an AIE Feature for Imaging Intracellular Drug Delivery. *Biomacromolecules* **2016**, *17*, 2920–2929.

(60) Zhao, H. J.; Li, Q.; Hong, Z. H. Paclitaxel-Loaded Mixed Micelles Enhance Ovarian Cancer Therapy through Extracellular pH-Triggered PEG Detachment and Endosomal Escape. *Mol. Pharmaceutics* **2016**, *13*, 2411–2422.

(61) Wang, B. D.; Xu, C. J.; Xie, J.; Yang, Z. Y.; Sun, S. H. pH Controlled Release of Chromone from Chromone-Fe<sub>3</sub>O<sub>4</sub> Nanoparticles. *J. Am. Chem. Soc.* **2008**, *130*, 14436–14437.

(62) Saito, H.; Hoffman, A. S.; Ogawa, H. I. Delivery of Doxorubicin from Biodegradable PEG Hydrogels Having Schiff Base Linkages. *J. Bioact. Compat. Polym.* **2007**, *22*, 589–601.

(63) Lv, P. P.; Ma, Y. F.; Yu, R.; Yue, H.; Ni, D. Z.; Wei, W.; Ma, G. H. Targeted Delivery of Insoluble Cargo (Paclitaxel) by PEGylated Chitosan Nanoparticles Grafted with Arg-Gly-Asp (RGD). *Mol. Pharmaceutics* **2012**, *9*, 1736–1747.

(64) Lai, C. H.; Chang, T. C.; Chuang, Y. J.; Tzou, D. L.; Lin, C. C. Stepwise Orthogonal Click Chemistry toward Fabrication of Paclitaxel/Galactose Functionalized Fluorescent Nanoparticles for HepG2 Cell Targeting and Delivery. *Bioconjugate Chem.* **2013**, *24*, 1698–1709.

(65) Kean, T.; Thanou, M. Biodegradation, Biodistribution and Toxicity of Chitosan. *Adv. Drug Delivery Rev.* **2010**, *62*, 3–11.

(66) Baldrick, P. The Safety of Chitosan as a Pharmaceutical Excipient. *Regul. Regul. Toxicol. Pharmacol.* **2010**, *56*, 290–299.

(67) Nam, H. Y.; Kwon, S. M.; Chung, H.; Lee, S. Y.; Kwon, S. H.; Jeon, H.; Kim, Y.; Park, J. H.; Kim, J.; Her, S.; Oh, Y. K.; Kwon, I. C.; Kim, K.; Jeong, S. Y. Cellular Uptake Mechanism and Intracellular Fate of Hydrophobically Modified Glycol Chitosan Nanoparticles. *J. Controlled Release* **2009**, *135*, 259–267.

(68) Lee, S. J.; Koo, H.; Jeong, H.; Huh, M. S.; Choi, Y.; Jeong, S. Y.; Byun, Y.; Choi, K.; Kim, K.; Kwon, I. C. Comparative Study of Photosensitizer Loaded and Conjugated Glycol Chitosan Nanoparticles for Cancer Therapy. *J. Controlled Release* **2011**, *152*, 21–29.

(69) Zhou, X.; Zhao, Y.; Chen, S. Y.; Han, S. L.; Xu, X. Q.; Guo, J. W.; Liu, M. Y.; Che, L.; Li, X. H.; Zhang, J. X. Self-Assembly of pH-Responsive Microspheres for Intestinal Delivery of Diverse Lipophilic Therapeutics. *Biomacromolecules* **2016**, *17*, 2540–2554.

(70) Zhong, Y. N.; Yang, W. J.; Sun, H. L.; Cheng, R.; Meng, F. H.; Deng, C.; Zhong, Z. Y. Ligand-Directed Reduction-Sensitive Shell-Sheddable Biodegradable Micelles Actively Deliver Doxorubicin into the Nuclei of Target Cancer Cells. *Biomacromolecules* **2013**, *14*, 3723–3730.